Comparison of Different Theories for Focusing through a Dielectric Interface.

Wiersma, S.H.; Torok, P.; Visser, T.D.; Varga, P.

published in
Journal of the Optical Society of America. A: Optics, image science, and vision.
1997

DOI (link to publisher)
10.1364/JOSAA.14.001482

document version
Publisher's PDF, also known as Version of record

Holographic approach to phase conjugation of optical near fields

Brian Vohnsen and Sergey I. Bozhevolnyi

Institute of Physics, Aalborg University, Pontoppidanstræde 103, DK-9220 Aalborg Øst, Denmark

Received August 29, 1996; revised manuscript received December 4, 1996; accepted December 19, 1996

Phase conjugation of optical dipole fields is considered in a static holographic scheme with totally internally reflected reference and reconstruction waves. It is shown that as the distance between the dipole object and the recording medium decreases from the far- to the near-field region, the intensity distribution of the reconstructed dipole field changes from a diffraction-limited light spot to a subwavelength-sized light spot that is brightest at the surface of the hologram. The influence of the thickness of the recording medium, the angle of incidence of the reconstruction wave, and the polarization configuration on the reconstructed intensity distribution are also discussed. © 1997 Optical Society of America [S0740-3232(97)02306-5]

1. INTRODUCTION

It has long been known that phase conjugation (PC) of an optical field can be accomplished by using a static hologram.[1] This type of hologram is obtained in two distinct stages. First, a photosensitive film is exposed to an interference pattern formed by light scattered by an object (the object wave) and a uniform reference wave. Second, the exposed film is appropriately processed, resulting in the static hologram. If the hologram is illuminated by the phase-conjugated reference wave, a phase-conjugated replica of the object wave is obtained. More recently, nonlinear optical techniques for PC have found widespread applications.[2] In such techniques the PC process occurs in real time, and it allows for an amplification of the phase-conjugated wave. Except for the scaling, the phase-conjugated wave is, in most cases, assumed to be an exact conjugate replica of the object wave with its propagation direction reversed.

Traditionally, evanescent components of the spectrum have been excluded from most theoretical studies of PC (see, for example, Ref. 2), but, seemingly, these are gaining more attention.[3–8] Recently, the first experimental evidences of PC of optical near fields (and consequently evanescent waves) have been reported.[9–11] One of the most interesting aspects of PC of evanescent waves is the possibility of focusing light beyond the classical Rayleigh–Abbé diffraction limit of approximately half the wavelength.[6–10]

The interest in PC of evanescent waves has, at least in part, emerged from the rapid development in both theoretical modeling and experimental techniques within near-field optics (some recent advances in this domain of optics can be found in Refs. 12 and 13). The most essential part of any optical near-field apparatus is a subwavelength-sized probe acting as an emitter and/or a detector of an optical near field while placed in the vicinity of the sample studied. In a particular configuration, the photon scanning tunneling microscope (PSTM),[14–16] the sample is placed in optical contact with the surface of, for example, a prism and illuminated by a totally internally reflected (TIR) wave. The light, which is scattered by the surface features of the sample, is then detected by a subwavelength-sized probe (typically an uncoated sharpened optical fiber tip), which is raster scanned at subwavelength distance (~5 nm) from the surface of the sample in order to retrieve an image. In static holography there exists a similar scheme with TIR reference and reconstruction waves that was introduced experimentally by Stetson in 1967.[17,18] Closely related techniques have been elaborated by Bryngdahl[19,20] and Nassenstein,[21] both of whom used evanescent reference and reconstruction waves (an overview of the subject can be found in Ref. 20). It is clear that if a small object is positioned sufficiently close to the recording medium in the above-mentioned scheme, the evanescent components of the object wave (which contain information about subwavelength-sized structures of the object) can be recorded. Thus, when the phase-conjugated reference wave is used for illuminating the resulting hologram, the reconstructed object wave will contain evanescent components, which may be detected by the near-field optical probe of the PSTM.

In continuation of our previous numerical studies of PC of optical near fields by means of a bulk phase-conjugating mirror,[6] we report, in the present paper, on a theoretical model of static holographic PC by using TIR reference and reconstruction waves. We suggest extending the holographic technique of Stetson for the recording of objects located at subwavelength distance from a thin photosensitive film. Preliminary results obtained with the proposed model have been published recently elsewhere.[7] The object in the present calculations is a point dipole that is driven coherently with the reference wave and located in the vicinity of the film [Fig. 1(a)]. The dashed curve in the figure serves to indicate that although a single point dipole has been chosen as the object, it could be a more complicated structure such as, for example, an uncoated fiber tip of a PSTM. When the distance between the dipole and the film is sufficiently small, the dipole near field (which includes evanescent components) can be recorded. The deformation of the dipole

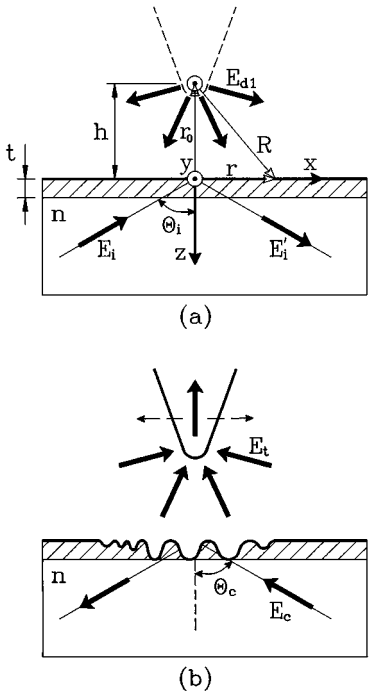

Fig. 1. Schematic representation of the holographic technique with TIR reference and reconstruction waves: (a) recording the field from a radiating dipole, (b) reconstruction and detection of the phase-conjugated replica of the dipole field.

field, as it penetrates the film, is incorporated into the description by applying the general Fresnel coefficients of the interface.[22] As a consequence, the interference between the dipole field *inside* the film and the TIR reference wave is considered. It is assumed that subsequent processing of the exposed film results in a thin surface hologram, with the topography modulation being linearly related to the exposure. For a processed film, in which the exposure results in a modulation of the refractive index, an equivalent surface profile can easily be determined if the modulation is small.[23] In the absence of the dipole object, the obtained hologram is subsequently illuminated by the phase-conjugated reference wave, whose diffraction creates a phase-conjugated replica of the dipole field above the hologram [Fig. 1(b)]. Owing to the close resemblance with the PSTM configuration, the near-field intensity distribution above the hologram can be evaluated with techniques widely used for PSTM modeling.[6,23–27] In the presence of an imaging probe, a simple dipolar model of the tip (with the detected signal being linearly proportional to the near-field intensity at the center of the tip) can provide some initial insights.[25] It should be stressed, however, that actual PSTM experiments may provide images that deviate significantly from near-field intensity distributions calculated in the absence of a probe. This is due to the nonnegligible size of any real probe currently employed.[6,27]

This paper is organized as follows. In Section 2 appropriate relations describing the holographic recording (Subsection 2.A) and the subsequent reconstruction (Subsection 2.B) of the dipole field are presented. Section 3 contains numerical results obtained with different system configurations when varying such parameters as the dipole–film separation, the thickness of the film, the angle of incidence of the reconstruction wave, and the field polarizations. In Section 4 we present our conclusions.

2. THEORETICAL DESCRIPTION

In the following, a model describing PC of a dipole field in a static holographic process is developed. First, the recording scheme is considered (Subsection 2.A), and, second (Subsection 2.B), the obtained hologram is illuminated in such a way that the phase-conjugated dipole field is formed.

A. Holographic Recording of the Dipole Field

The system under consideration consists of a point dipole situated at $\mathbf{r}_0$ in vacuum above a thin photosensitive film deposited onto a substrate of equal refractive index n [Fig. 1(a)]. The dipole is driven by the monochromatic field $\mathbf{E}_0(\mathbf{r}_0)$ with wavelength λ [the origin of this field, which for simplicity is not shown in Fig. 1(a), is discussed in Subsection 2.B]. A hologram is being recorded in the film by means of interference between the induced dipole field $\mathbf{E}_{d2}(\mathbf{r})$ and a reference wave $\mathbf{E}_r(\mathbf{r})$, the latter being the sum of a plane wave $\mathbf{E}_i(\mathbf{r})$ incident from below (at an angle θ_i larger than the critical one) and the corresponding TIR wave $\mathbf{E}_i'(\mathbf{r})$. The TIR configuration eliminates the transmission of a homogeneous wave, which would affect the dipole radiation, and it facilitates the subsequent detection process of phase-conjugated light [Fig. 1(b)]. Electromagnetic coupling between the dipole and the film–substrate system can be neglected for large distances $h \gg \lambda$. For smaller distances $h \ll \lambda$, the coupling may not be negligible, resulting in an increase of the power radiated by the dipole,[28] and configurational resonances may appear.[29] Nevertheless, for both dielectric substrate and dipole, the coupling is in general small.[25] It should be kept in mind that the film surface is assumed to be perfectly flat during the exposure, and only *after* development (in the absence of light) of the exposed film is the topography-modulated surface hologram obtained. If the modulation had occurred *during* the exposure, it could have resulted in an increased coupling and a strong modification of the emitted dipole field. This would have required a more refined self-consistent approach (for a fuller discussion on the influence of coupling, see the recent review by Girard and Dereux[30] and the references therein). For convenience we consider here the case of negligible coupling, since it simplifies the following calculations considerably. Consequently, the dipole field above the film, $\mathbf{E}_{d1}(\mathbf{r})$, can be written as[29]

$$\mathbf{E}_{d1}(\mathbf{r}) = -\frac{\alpha}{4\pi\epsilon_0}\left(k_1^2\,\frac{\mathbf{RR}-R^2\mathbf{U}}{R^3} + ik_1\,\frac{3\mathbf{RR}-R^2\mathbf{U}}{R^4} - \frac{3\mathbf{RR}-R^2\mathbf{U}}{R^5}\right)\cdot\mathbf{E}_0(\mathbf{r}_0)\exp(ik_1R), \tag{1}$$

where $\mathbf{R} = \mathbf{r} - \mathbf{r}_0$, $R = |\mathbf{R}|$, and $\mathbf{U}$ is the unit tensor. The wave numbers of light above and in the film are denoted by $k_1 = 2\pi/\lambda$ and $k_2 = 2\pi n/\lambda$, respectively. In Eq. (1) we have used the isotropic Rayleigh polarizability

$\alpha = 4\pi\epsilon_0 a^3(n_d{}^2 - 1)/(n_d{}^2 + 2)$, which is valid for subwavelength-sized (dielectric) scatterers with radius $a \ll \lambda$ and refractive index n_d. The vacuum permittivity is denoted by ϵ_0. The first, second, and third terms in Eq. (1) denote, respectively, the far, middle, and near fields of the dipole radiation. The field $\mathbf{E}_{d1}$, however, is not the one recorded, since, on penetrating the film, it is modified in accordance with the Fresnel coefficients of the interface. This can be taken into account by making a plane-wave decomposition of $\mathbf{E}_{d1}$ just above the film ($z = 0^-$), resulting in the corresponding spectrum

$$\boldsymbol{\epsilon}_{d1}(u, v) = \int\int_{-\infty}^{\infty} \mathbf{E}_{d1}(x, y, z = 0^-) \times \exp[-i(ux + vy)]\mathrm{d}x\mathrm{d}y. \quad (2)$$

Inside the film this spectrum is modified by the Fresnel transmission matrix[22] $\mathbf{T}_{1,2}$ as

$$\boldsymbol{\epsilon}_{d2}(u, v) = \mathbf{T}_{1,2}(u, v) \cdot \boldsymbol{\epsilon}_{d1}(u, v), \quad (3)$$

where $\mathbf{T}_{1,2}$ can modify the spectrum considerably, as shown in Fig. 2(a), in particular for the components that are propagating within the film [i.e., for $|\mathbf{k}_\parallel| \leqslant k_2$, where $\mathbf{k}_\parallel = (u, v)$ is the projection of the wave vector onto the film surface]. Furthermore, $\mathbf{T}_{1,2}$ leads to a mixing of the various polarization components of the dipole field. From the spectrum $\boldsymbol{\epsilon}_{d2}$, the dipole field $\mathbf{E}_{d2}$ just inside the film ($z = 0^+$) can be written as

$$\mathbf{E}_{d2}(x, y, z = 0^+) = \frac{1}{4\pi^2}\int\int_{-\infty}^{\infty} \boldsymbol{\epsilon}_{d2}(u, v) \times \exp[i(ux + vy)]\mathrm{d}u\mathrm{d}v. \quad (4)$$

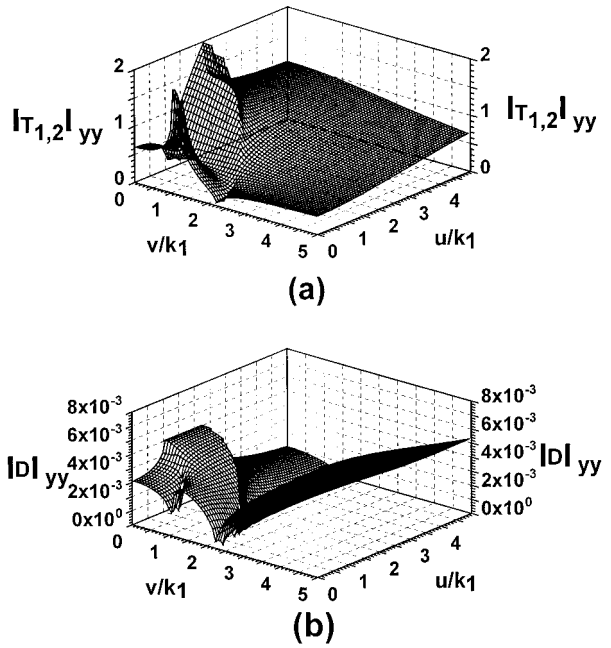

Fig. 2. Modulus of the yy term of (a) the transmission matrix from vacuum to film and (b) the diffraction matrix from film to vacuum. In both calculations $n = 2.2$ and $\lambda = 633$ nm have been used.

If the subsequent processing of the thin film (with thickness $t \ll \lambda/n$) is linear with respect to the exposure and $|\mathbf{E}_{d2}| \ll |\mathbf{E}_r|$ is satisfied, the topography modulation is governed by the interference terms $\mathbf{E}_r \cdot \mathbf{E}_{d2}^* + \mathbf{E}_r^* \cdot \mathbf{E}_{d2}$. It should be mentioned that the constant intensity term $|\mathbf{E}_r|^2$ is omitted, since it does not modulate the surface profile but merely changes the overall thickness of the processed film. It is clear that highly evanescent components of the dipole spectrum inside the film do not modify the topography significantly, on account of their limited penetration depth. In the linear regime of film processing, this can be taken into account by integrating the field intensity, for each individual component, across the thickness of the film. Such a procedure results in the following weighting function $g(u, v)$ of the dipole spectrum:

$$g(u, v) = \begin{cases} 1 & \text{if } |\mathbf{k}_\parallel| \leqslant k_2 \\ \dfrac{1 - \exp(-|w_2|t)}{|w_2|t} & \text{otherwise} \end{cases}, \quad (5)$$

where $w_2(u, v) = (k_2{}^2 - |\mathbf{k}_\parallel|^2)^{0.5}$. The reference wave for the recording is obtained by means of a plane wave [Fig. 1(a)]: $\mathbf{E}_i = \mathbf{E}_i^0 \exp[i(u_i x + w_i z)]$, thus providing the reference field at $z = 0^+$ as

$$\mathbf{E}_r(x, y, z = 0^+) = \mathbf{E}_r^0 \exp(iu_r x), \quad (6)$$

with $u_r = u_i = k_2 \sin\theta_i$ and $w_i = -k_2 \cos\theta_i$. The spectrum of the incident wave, $\boldsymbol{\epsilon}_i$, and of the reference field, $\boldsymbol{\epsilon}_r$, are related through $\boldsymbol{\epsilon}_r = (\mathbf{U} + \mathbf{T}_{2,2}) \cdot \boldsymbol{\epsilon}_i$, where the matrix $\mathbf{T}_{2,2}$ consists of the reflection coefficients of the interface, which accounts for the TIR field $\mathbf{E}_i'$. The topography modulation $f(x, y)$ of the resulting hologram (obtained after the development of the exposed film) can be expressed from Eqs. (4)–(6) in the following form:

$$f(x, y) = \frac{\gamma t}{4\pi^2}\int\int_{-\infty}^{\infty}\{\mathbf{E}_r^0 \cdot \boldsymbol{\epsilon}_{d2}^*(-u, -v) \times \exp[i(u + u_r)x] + \mathbf{E}_r^{0*} \cdot \boldsymbol{\epsilon}_{d2}(u, v) \times \exp[i(u - u_r)x]\}g(u, v)\exp(ivy)\mathrm{d}u\mathrm{d}v, \quad (7)$$

where the asterisk denotes the complex-conjugated quantity and γ is a scaling factor of the modulation. Consequently, the corresponding spectrum $F(u, v)$ of the surface profile can be written as

$$F(u, v) = \gamma t[g(u - u_r, v)\mathbf{E}_r^0 \cdot \boldsymbol{\epsilon}_{d2}^*(-(u - u_r), -v) + g(u + u_r, v)\mathbf{E}_r^{0*} \cdot \boldsymbol{\epsilon}_{d2}(u + u_r, v)]. \quad (8)$$

It can be seen that the spectrum of the surface profile contains two distinct terms: One is the phase-conjugated dipole spectrum (inside the film) centered at $u = u_r$, and the other is the unconjugated dipole spectrum (inside the film) centered at $u = -u_r$. It is informative to note from Eqs. (7) and (8) that neither of these spectra is perfectly encoded into the surface profile. Clearly, both of them are scaled by their respective weighting function, but, furthermore, the scalar products $\mathbf{E}_r^0 \cdot \boldsymbol{\epsilon}_{d2}^*$ and $\mathbf{E}_r^{0*} \cdot \boldsymbol{\epsilon}_{d2}$ show that only parts of these spectra are actually encoded. Only that part of the dipole field whose polariza-

tion coincides with that of the reference wave contributes to the topography modulation. Consequently, in the subsequent reconstruction process, the dipole field can be only partially reconstructed from the hologram. When the dipole is located far from the film, it is to be anticipated that the best results can be achieved with an s-polarized reference wave, where only the y component of the dipole field is recorded. With a p-polarized reference wave, *both* x and z components of the dipole field contribute to the topography modulation (with a weighting dependent on n and θ_i), and as a result of the polarization mixing, a poorer reconstruction than in the case of s polarization should be anticipated.

B. Reconstruction of the Dipole Field

The obtained surface hologram is illuminated from below [Fig. 1(b)] by the plane wave $\mathbf{E}_c = \mathbf{E}_c^0 \exp[i(u_c x + w_c z)]$, where $u_c = -k_2 \sin\theta_c$ and $w_c = -k_2 \cos\theta_c$. To calculate the spectrum of the transmitted field $\mathbf{E}_t$, we adopt the perturbative technique extensively used and studied in relation to near-field optics (see Refs. 23–27 and the references therein). The perturbative technique has been found accurate for shallow surfaces with the variation in height $\Delta z \leqslant \lambda/20$ and with spatial frequencies $|\mathbf{k}_\parallel| \ll 1/\Delta z$.[23] Within this approximation the spectrum of the transmitted field can be written as[26]

$$\boldsymbol{\epsilon}_t(u, v) = \{\boldsymbol{\epsilon}_{t0} + i(n^2 - 1)\mathbf{D}(u, v) \cdot [F(u - u_c, v)\mathbf{T}_{2,1}(u_c, 0) \cdot \mathbf{E}_c^0]\}\exp(iw_1 z), \tag{9}$$

where $w_1(u, v) = -(k_1{}^2 - |\mathbf{k}_\parallel|^2)^{0.5}$, $\boldsymbol{\epsilon}_{t0} = \mathbf{T}_{2,1} \cdot \boldsymbol{\epsilon}_c$ is the spectrum of the undiffracted transmitted field $\mathbf{E}_{t0}$ corresponding to an unmodulated interface [cf. Eq. (3)], $\boldsymbol{\epsilon}_c$ is the spectrum of the reconstruction wave, and $\mathbf{T}_{2,1}$ is the Fresnel transmission matrix[22] from film to vacuum. The matrix $\mathbf{D}$ is a diffraction matrix derived by virtue of the boundary conditions for the fields when taking the actual surface profile into account. Consequently, the distribution of the transmitted field $\mathbf{E}_t$ at a given height above the hologram can be found as the inverse Fourier transform of $\boldsymbol{\epsilon}_t$ as in Eq. (4). Notice from this and Eq. (9) that the transmitted field can be considered as the sum of an undiffracted field $\mathbf{E}_{t0}$ (first term) and a diffracted field $\mathbf{E}_{td}$ (second term).

Combining Eqs. (8) and (9) for a configuration with the hologram illuminated by a wave having $u_c = -u_r$ (the conjugated reference wave) results in

$$\boldsymbol{\epsilon}_t(u, v) = \{\boldsymbol{\epsilon}_{t0} + i(n^2 - 1)\gamma t[g(u, v)\mathbf{E}_r^0 \cdot \boldsymbol{\epsilon}_{d2}^*(-u, -v) + g(u + 2u_r, v)\mathbf{E}_r^{0*} \cdot \boldsymbol{\epsilon}_{d2}(u + 2u_r, v)] \times \mathbf{D}(u, v) \cdot \mathbf{T}_{2,1}(-u_r, 0) \cdot \mathbf{E}_c^0\}\exp(iw_1 z). \tag{10}$$

For $\mathbf{E}_c^0 \propto \mathbf{E}_r^{0*}$ it can be seen from Eq. (10) that the phase-conjugated dipole spectrum $\boldsymbol{\epsilon}_{d2}^*$ has been reconstructed. Along with this, however, the unconjugated dipole spectrum $\boldsymbol{\epsilon}_{d2}$ has also been reconstructed, but the latter is shifted by $-2u_r$. The occurrence of two images (corresponding to the ± 1st diffraction orders) in the reconstruction from a thin hologram has been known since the onset of holography.[31,32] In conventional (far-field) holography, these two images can be spatially separated by recording with angular separated reference and object waves.[33] In comparison with this, recording and reconstruction with TIR waves have the further advantage that all the propagating components belonging to the shifted spectrum (here $\boldsymbol{\epsilon}_{d2}$) are converted to evanescent waves in the reconstruction. In particular, for large angles of incidence θ_c, the field that corresponds to the shifted part of the spectrum will be strongly confined to the interface. This can be seen from the exponential factor in Eq. (10), since w_1 becomes imaginary for the main part of the shifted spectrum.

As discussed in Subsection 2.A, the loss of polarization information during the recording reduces the quality of the PC. Another factor with a deteriorating effect is the double passage of the vacuum–film boundary and the resulting deformations of the spectrum induced by $\mathbf{T}_{1,2}$, $\mathbf{T}_{2,1}$, and $\mathbf{D}$ (see Fig. 2). Furthermore, at $h \ll \lambda$ interference between the undiffracted field $\mathbf{E}_{t0}$ and the diffracted field $\mathbf{E}_{td}$ can influence the intensity distribution of the transmitted field, so that it deviates significantly from the phase-conjugated contribution. Such interference has been observed experimentally in PSTM experiments under similar conditions to those depicted in Fig. 1(b) (see, for instance, Ref. 34, in which the near-field optical images are related to scattering of light by subwavelength-sized particles deposited onto an otherwise flat substrate). Another factor in this context is the difference in phase between the reference field $\mathbf{E}_r$ and the dipole field $\mathbf{E}_{d2}$ that is encoded into the hologram. Clearly, the intensity distribution of the transmitted field is sensitive to changes in phase of either $\mathbf{E}_r$ or $\mathbf{E}_{d2}$. For a dipole situated at $h > \lambda$ during the recording, the aforementioned interference during the reconstruction between the undiffracted and diffracted fields is negligible (because of the evanescent decay of the reconstruction wave above the hologram). At smaller recording distances, the sensitivity to phase shifts can be circumvented by letting the dipole be driven by the evanescent tail of the reference wave above the film. Such an "in-phase" recording is also attractive in terms of coherence requirements for the reference wave on account of the smallness of the distances involved. Finally, notice that when illuminating the hologram with $u_c = u_r$ and $\mathbf{E}_c^0 \propto \mathbf{E}_r^0$ (i.e., the same wave used both for reference and for reconstruction), one can write an equation similar to Eq. (10). In such a case, it can be deduced that the unconjugated dipole field (the mirror image of the dipole) is reconstructed, whereas the spectrum of the phase-conjugated dipole field is shifted by $+2u_r$ and correspondingly attenuated in the transmitted field above the hologram.

3. NUMERICAL RESULTS

On the basis of the model discussed in Section 2, we have performed various numerical calculations for different configurations of the system. In the results presented, the following parameters have been used: $\lambda = 633$ nm, $\theta_i = \theta_c = 60°$ (with the exception of Fig. 8 below), and $n = 2.2$ (corresponding to the refractive index of the $LiNbO_3$ crystal used in our previous experimental

work[9–11]). The thickness of the film has been chosen as $t = 10$ nm (with the exception of Fig. 7 below), and the scaling factor γ has been chosen separately in each case so that the maximum topography modulation equals t. As discussed in Subsection 2.B, the maximum modulation thickness sets an upper limit on the spatial frequencies, which, for the chosen parameters, become $|\mathrm{k}_\parallel| \ll 1/t \approx 10k_1$, in order to yield reliable results with the perturbative diffraction technique.[23] This means, in turn, a limitation of the smallest distance between the dipole and the film that can be used in our model. Consequently, $|\mathrm{k}_\parallel| = 10k_1$ has been chosen as the upper frequency limit in the calculations, so that the validity of the perturbation condition can be estimated. The polarizability α of the dipole situated at $\mathrm{r}_0 = (0,0,-h)$ has been kept constant in the present calculations. The chosen value corresponds to a dielectric particle with $a = 50$ nm and $n_d = 1.5$, but it could equally well be any other particle with the same polarizability (for instance, a gold particle with $a = 30$ nm would have approximately the same polarizability at the chosen wavelength), since this is the only particle parameter that enters in the scaling of the dipole field [cf. Eq. (1)]. The influence of the imaginary part of the polarizability has been discussed in a previous paper.[7]

First, a recording configuration with the dipole situated at $h = 30$ nm above the film and driven by the evanescent tail of an s-polarized TIR reference wave has been considered. In this case the y component of the dipole radiation is dominant, and appropriate spectra for various stages of the process are pictured in Fig. 3. The spectrum component $\boldsymbol{\epsilon}_{d1,y}$ of the incident dipole field is particularly strong in the direction perpendicular to the dipole axis at $|u| \approx k_1$, but at this small distance it certainly also contains a large number of evanescent waves [Fig. 3(a)]. In the spectrum component $\boldsymbol{\epsilon}_{d2,y}$ of the dipole field inside the film, however, the $|u| \approx k_1$ components are suppressed (related to the fact that the reflectivity is close to 1 at an oblique angle of incidence), whereas components for which $|u| \approx k_2$ are somewhat enhanced [Fig. 3(b)]. This can also be seen by the behavior of the $(\mathbf{T}_{1,2})_{yy}$ term of the transmission matrix [Fig. 2(a)]. On reconstruction with the phase-conjugated reference wave, the spectrum component $\boldsymbol{\epsilon}_{td,y}$ of the diffracted field just above the hologram ($z = 0^-$) contains both the phase-conjugated and unconjugated parts [Fig. 3(c)] as discussed in Subsection 2.B. The unconjugated dipole spectrum, however, is shifted by $2u_c$ to the evanescent region and attenuated on account of the $\mathbf{D}_{yy}$ matrix component [Fig. 2(b)]. Finally, the spectrum of the diffracted field in the plane of the dipole ($z = -30$ nm) consists mainly of the phase-conjugated dipole spectrum [Fig. 3(d)]. This image clearly shows the effect of low-pass filtering [cf. Eq. (10)], although at this small distance the evanescent components with $|\mathbf{k}_\parallel| < k_2$ largely remain.

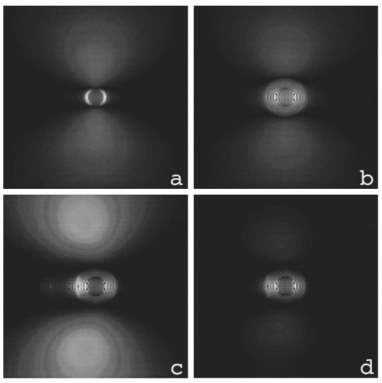

Fig. 3. Linear gray-scale representations (horizontally $u_{\max} = 10k_1$ and vertically $v_{\max} = 10k_1$) of the modulus of the dipole spectrum (y component) at various stages of the process: (a) outside the film ($z = 0^-$), (b) inside the film ($z = 0^+$), (c) diffracted ($z = 0^-$), and (d) diffracted ($z = -h$). The dipole is situated at $h = 30$ nm in front of the film during the recording.

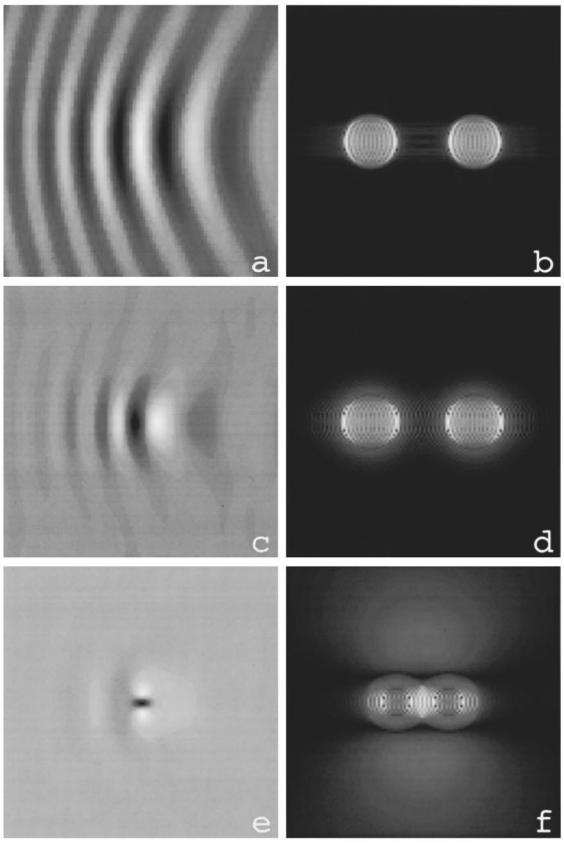

Fig. 4. Linear gray-scale representations (x axis is horizontal, and y axis is vertical) [(a), (c) 2 μm × 2 μm; (e) 1 μm × 1 μm and (b), (d) $u_{\max} = 5k_1$, $v_{\max} = 5k_1$; (f) $u_{\max} = 10k_1$, $v_{\max} = 10k_1$] of (a), (c), (e) the recorded holograms and (b), (d), (f) the modulus of their corresponding Fourier spectra for three different configurations [(a), (b) $h = 600$ nm; (c), (d) $h = 150$ nm; and (e), (f) $h = 30$ nm], all obtained with an s-polarized reference wave and dipole.

For the same configuration as that considered above, but for various distances between the dipole and the film, the topography modulation $f(x,y)$ of the recorded hologram and its corresponding spectrum $F(u,v)$ have been evaluated in Fig. 4 for three different situations: (a), (b) $h = 600$ nm; (c), (d) $h = 150$ nm; and (e), (f) $h = 30$ nm (identical to the configuration used in Fig. 3). In the first case, the dipole field that reaches the film is governed by the far-field term in Eq. (1). Accordingly, the recorded field is dominated by interference fringes [Fig. 4(a)] on account of the field retardation factor $\exp(ik_1R)$. The fact that mostly propagating components reach the film can be

seen from the surface spectrum [Fig. 4(b)], which is largely confined within two separate circles of radius k_1. The occurrence of two distinct spectra in the surface and their interpretation have been discussed in Subsection 2.A [cf. Eq. (8)]. In the second case, the middle field influences the recording more, since at this distance the far- and near-field terms partly cancel out. Furthermore, at distances $R \ll \lambda$ the retardation is of much less importance, and therefore the profile contains fewer interference fringes [Fig. 4(c)]. The corresponding surface spectrum [Fig. 4(d)] shows that also components with $k_1 < |\mathbf{k}_\parallel| < k_2$ (i.e., evanescent above but propagating inside the film) have partly been recorded. For the third case, the near-field term in Eq. (1) is dominant, and the recorded hologram is mostly restricted to the region just below the dipole [Fig. 4(e)]. The corresponding surface spectrum [Fig. 4(f)] shows that at this distance the components that are evanescent inside the film also affect the recording. Note that the chosen angle of incidence ($\theta_i = 60°$) is no longer sufficiently large to effectively separate the unconjugated from the phase-conjugated dipole spectrum.

In the reconstruction the field $\mathbf{E}_t$ transmitted through the hologram has been evaluated in the plane of the dipole ($z = -h$), and the intensity $|\mathbf{E}_t|^2$ is shown in Fig. 5

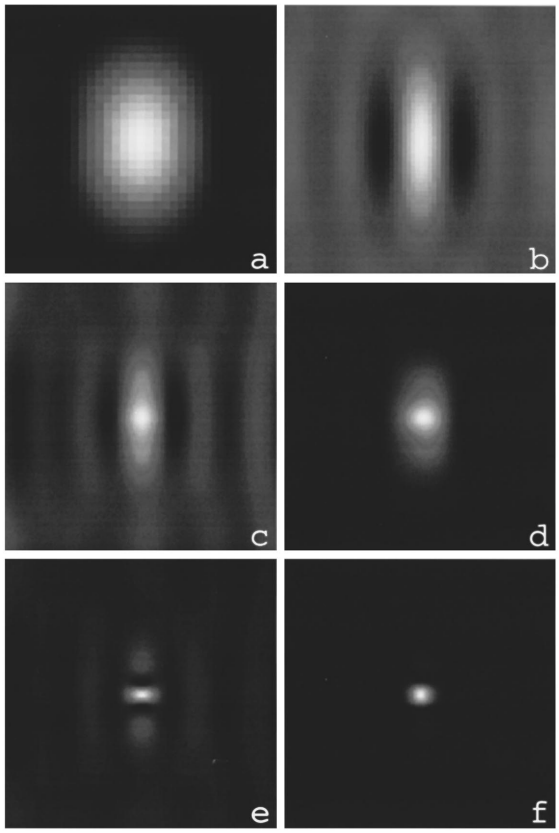

Fig. 5. Linear gray-scale representations ($1\ \mu\text{m} \times 1\ \mu\text{m}$) of the transmitted field intensity with (a) $h = 600$ nm; (b) $h = 150$ nm; (c), (d) $h = 60$ nm; and (e), (f) $h = 30$ nm; all obtained with an s-polarized reference and reconstruction wave and dipole. The undiffracted field $\mathbf{E}_{t0}$ has been omitted in (d) and (f). The image contrast, i.e., the relative difference between the maximum and minimum intensities, is (a) 100%, (b) 63%, (c) 19%, (d) 100%, (e) 10%, and (f) 100%.

for the following situations: (a) $h = 600$ nm; (b) $h = 150$ nm; (c), (d) $h = 60$ nm; and (e), (f) $h = 30$ nm. It is found that, in the far-field region ($h \gg \lambda/2\pi$), the size of the conjugated light spot is in good agreement with the classical diffraction limit ($\sim\lambda/2$), although the spot is rather elongated [Fig. 5(a)]. This asymmetry of the light spot is caused by the different radiative properties of a dipole along and perpendicular to its axis. At the intermediate distances, the light spot is somewhat smaller [Figs. 5(b)–5(d)], mainly because of the recorded evanescent waves [cf. Fig. 4(d)]. Along the x axis, however, the smaller size is also a result of destructive interference between the undiffracted (evanescent) $\mathbf{E}_{t0}$ part and the diffracted $\mathbf{E}_{td}$ part of the transmitted field. This can be seen by comparing Figs. 5(c) and 5(d), where $\mathbf{E}_{t0}$ has been omitted in the latter. For instance, for $\theta_c = 60°$ the penetration depth of the undiffracted field is ~ 62 nm, at which distance it is still comparable in magnitude with the diffracted field. At even smaller distances ($h \ll \lambda/2\pi$), the size of the light spot decreases significantly [Figs. 5(e) and 5(f)] on account of a strong influence of evanescent waves during both the recording and the reconstruction processes [cf. Fig. 4(f)]. At such small distances from the surface, the diffracted field is very intense just below the former position of the dipole, and the aforementioned interference with the undiffracted field is therefore of less influence on the size of the light spot. This can be seen by comparing Figs. 5(e) and 5(f), where $\mathbf{E}_{t0}$ has been omitted in the latter. Notice the different orientation of the slightly elongated near-field light spot [Fig. 5(f)] compared with that of the far-field light spot [Fig. 5(a)], which is related to the difference in the angular distribution of the far and near fields of a dipole.

Cross sections (at $x = 0$ and $y = 0$) showing the diffracted field during the reconstruction are presented in Fig. 6 (the undiffracted field has been omitted for ease of view) for the following configurations: (a), (b) $h = 600$ nm; (c), (d) $h = 300$ nm; and (e), (f) $h = 150$ nm. At the largest distance, the phase-conjugated field forms a well-defined light spot separated from the hologram [Figs. 6(a) and 6(b)]. At the intermediate distance, the light spot is not completely separated from the hologram [Figs. 6(c) and 6(d)], and interference just above the hologram between the phase-conjugated and the unconjugated dipole field can be seen [cf. Eq. (10)]. At the even smaller distance, the maximum of the phase-conjugated light spot is no longer separated from the interface [Figs. 6(e) and 6(f)], because of the influence of evanescent waves in the PC process. This is caused by the change of the decay direction for evanescent waves that undergo PC.[3]

The thickness of the film is an important parameter and enters not only as a scaling factor of the diffracted field in Eq. (10) but also in the weighting function $g(u,v)$ of the evanescent waves as shown in Eq. (5). To examine the influence of $g(u,v)$ on the reconstruction process, we have calculated the light diffracted by the hologram $\mathbf{E}_{td}$ at $z = -30$ nm for the same configuration as that considered in Fig. 5(f) when varying the thickness of the film. Increasing the thickness results in a stronger filtration of evanescent waves [cf. Eq. (5)] and consequently in a larger light spot during the reconstruction as

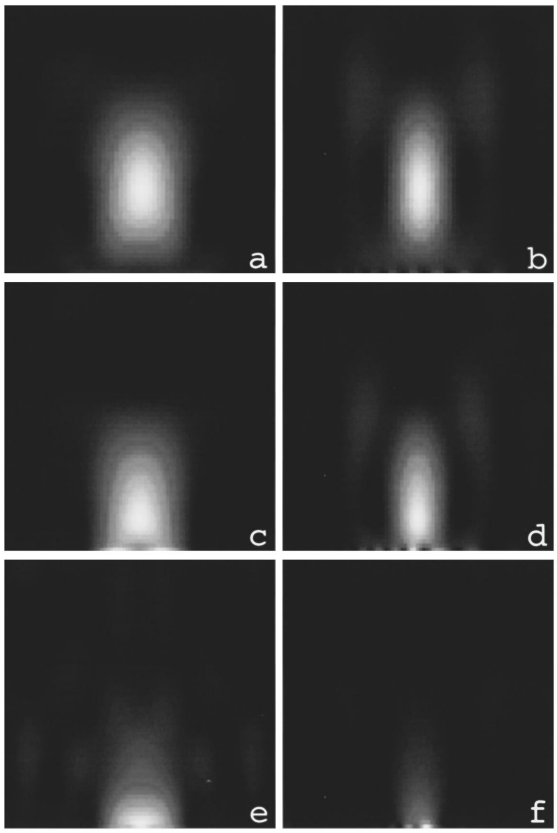

Fig. 6. Linear gray-scale representations ($2\ \mu m \times 2\ \mu m$) of the diffracted field intensity in the cross sections (a), (c), (e) $x = 0$ and (b), (d), (f) $y = 0$. The images correspond to (a), (b) $h = 600$ nm; (c), (d) $h = 300$ nm; and (e), (f) $h = 150$ nm, all obtained with an s-polarized reference and reconstruction wave and dipole. The hologram coincides with the lower boundary of the images.

shown in Fig. 7, which is more reminiscent of the far-field light spot shown in Fig. 5(a). Accordingly, it appears that, for studying PC of optical near fields with static holography, thin films are most adequate.

We have, furthermore, examined the sensitivity of the reconstructed field to angular misalignments of the reconstruction wave in the same recording configuration as that considered above. The results obtained are shown in Fig. 8. By comparison with Fig. 5(e), it can be seen that for closely spaced dipole and film the reconstructed light spot is highly insensitive to such misalignments ($\pm 10°$). On the other hand, if the reconstruction scheme is inverted so that the same wave is used both as reference and for reconstruction (i.e., $\theta_c = -\theta_i = -60°$), then the unconjugated dipole field is reconstructed as discussed at the end of Subsection 2.B. Because of the influence of evanescent components, the diffracted field forms a double subwavelength-sized light spot in the near-field image as shown in Fig. 8(c), whereas at a further distance the intensity distribution shown in Fig. 8(d) becomes more similar to the far-field radiation pattern of a dipole.

As discussed at the end of Subsection 2.A, recording the dipole radiation with a p-polarized reference wave is expected to reduce the quality of the reconstructed light spot. To pursue this issue further, we have considered a configuration identical to that used in the calculation of the images in Fig. 5, with the only exception being that both the recording and reconstruction waves are p polarized. The dipole is driven by an external source in such a way that the dipole is polarized along the z axis (this orientation of the dipole cannot alone be achieved by the transmitted evanescent tail of the reference wave). The resulting phase-conjugated light spots at various distances are shown in Fig. 9. Indeed, at larger distances [Figs. 9(a)–9(d)] no simple image appears, in accordance with the predictions, and the images are highly influenced by interference between the undiffracted and diffracted fields [compare Figs. 9(c) and 9(d)]. However, at very small distances a single subwavelength-sized light spot appears [Figs. 9(e) and 9(f)]. This is most apparent if the undiffracted field is omitted [Fig. 9(f)], resulting in a light spot much like the one obtained with s-polarized light [cf. Fig. 5(f)]. The successful PC of the dipole near field for both s and p polarizations is related to the fact that at distances $h \ll \lambda/2\pi$ the near-field part of the dipole field is very intense just beneath the dipole [i.e.,

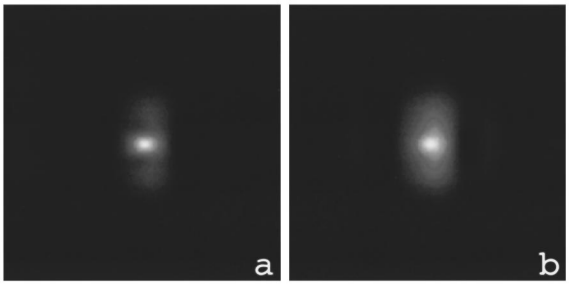

Fig. 7. Linear gray-scale representations ($1\ \mu m \times 1\ \mu m$) of the diffracted field intensity for $z = -h = -30$ nm with (a) $t = 100$ nm and (b) $t = 300$ nm, all obtained with an s-polarized reference and reconstruction wave and dipole.

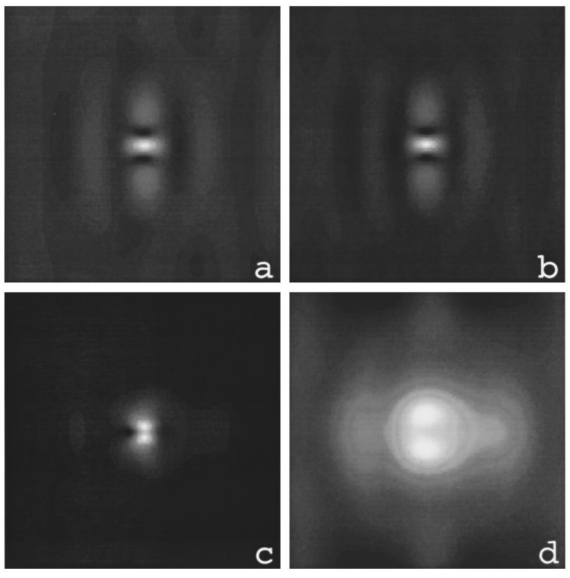

Fig. 8. Linear gray-scale representations ($1\ \mu m \times 1\ \mu m$) of the transmitted field intensity at $z = -h = -30$ nm with (a) $\theta_c = 50°$ and (b) $\theta_c = 70°$ and of the diffracted field intensity for $\theta_c = -60°$ and $h = 30$ nm at (c) $z = -30$ nm and (d) $z = -120$ nm, all obtained with an s-polarized reference and reconstruction wave and dipole.

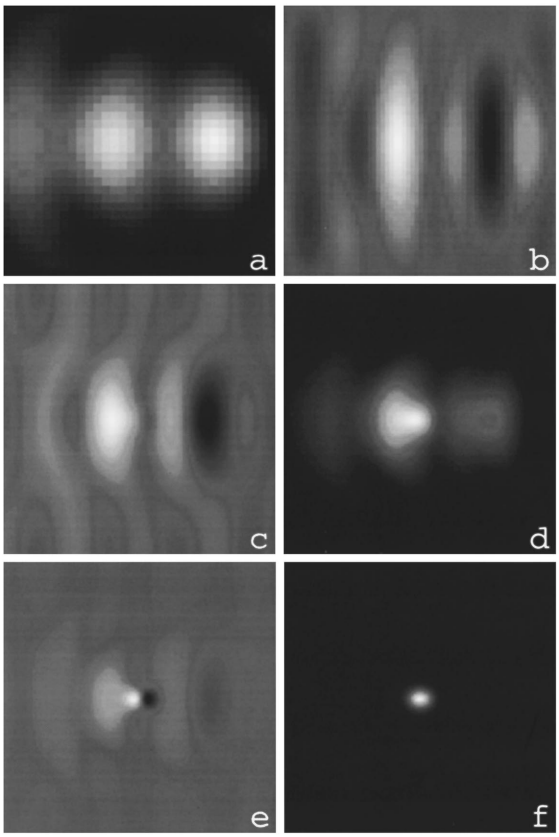

Fig. 9. Linear gray-scale representations (1 μm $\times$ 1 μm) of the transmitted field intensity obtained with a p-polarized reference and reconstruction wave and a z-polarized dipole. The image contrast is (a) 100%, (b) 86%, (c) 15%, (d) 100%, (e) 5%, and (f) 100%. Other details are the same as those of Fig. 5.

where R is smallest; cf. Eq. (1)] and the near-field hologram is, therefore, mainly confined to this region as shown in Fig. 4(e). For a dipole oriented along the z axis, this is the region where the z-polarized near-field component prevails, and, accordingly, the mixing of polarizations (as is present in the far-field case) is small.

4. CONCLUSIONS

In this paper we have investigated PC of optical fields in a static holographic process with TIR reference and reconstruction waves. In particular, PC of optical near fields, which relates to our previous experimental studies,[9–11] has been addressed. A single point dipole driven by a monochromatic field has been chosen as the source of radiation. The three distinct contributions to the dipole field (far-, middle-, and near-field) [cf. Eq. (1)] have all been included in the calculations, although special attention has been paid to the near-field part. Because of the similarity between the holographic reconstruction process with a TIR wave and the PSTM technique, the first-order diffraction theory[23–27] often used in the latter has been used in the calculations.

Several important issues about the proposed holographic PC technique have been examined and clarified. The importance of taking the refractive index of the film into account has been demonstrated through calculations that show the deformation of the dipole spectrum both when the field penetrates into the film and in the subsequent PC process. It has been found that for large distances ($h > \lambda$) between the dipole and the film during the recording, the resulting hologram can provide a diffraction-limited light spot of the phase-conjugated dipole field. At smaller distances ($h \ll \lambda$), the extent of the phase-conjugated light spot becomes smaller because of the influence of evanescent components. In this case the phase-conjugated dipole field results in a subwavelength-sized light spot that is brightest just in front of the hologram (and not at the origin of the point dipole) as a result of the symmetry properties of phase-conjugated evanescent waves.[3,6] During the recording it has been found to be preferable to excite the dipole (in phase) with the evanescent tail of an s-polarized reference wave and subsequently reconstruct the dipole field with the phase-conjugated reference wave. In the case of p-polarized reference and reconstruction waves, mixing of the polarization components may result in ambiguous images. Owing to the TIR configuration, the simultaneously reconstructed unconjugated dipole field remains closely confined to the surface of the hologram, thus interfering only slightly with the phase-conjugated dipole field. Additionally, the reconstruction has been found to be highly insensitive to misalignments of the reconstructing TIR wave. Naturally, the model described is not limited to a single point dipole; the principle can be extended to treat more complicated objects, for instance by dividing them into a set of elementary scatterers.

To study PC of evanescent waves in optical near fields by this holographic technique, the recording medium should preferably be thin ($<$100 nm), so that homogeneous waves do not dominate the phase-conjugated field. Furthermore, computer generation of the holograms might prove advantageous, since, in this case, the troublesome recording with, for example, the optical probe of a PSTM[9–11] can be avoided. Nonlinear techniques may be even more fruitful for PC of optical near fields in thin films, partly because the interaction length (and consequently the PC reflectivity) will then be largest for evanescent waves, since these propagate along the interface. In the context of data storage by near-field optical means, holographic PC for obtaining subwavelength-sized light spots might be superior to scattering of light by subwavelength-sized obstacles.[12,13,35] In particular, this may be the case for nonlinear techniques, where an amplification of the phase-conjugated wave may allow for an improved signal-to-noise ratio.

REFERENCES

1. H. Kogelnik, “Holographic image projection through inhomogeneous media,” Bell Syst. Tech. J. **44**, 2451–2455 (1965).
2. B. Ya. Zel’dovich, N. F. Pilipetsky, and V. V. Shkunov, *Principles of Phase Conjugation* (Springer-Verlag, Berlin, 1985).
3. M. Nieto-Vesperinas and E. Wolf, “Phase conjugation and symmetries with wave fields in free space containing evanescent components,” J. Opt. Soc. Am. A **2**, 1429–1434 (1985).
4. M. Nieto-Vesperinas, *Scattering and Diffraction in Physical Optics* (Wiley-Interscience, New York, 1991), Chap. 8.
5. G. S. Agarwal and S. D. Gupta, “Evanescent coupling of a

dipole to a phase conjugate mirror," Opt. Commun. **119**, 591–596 (1995).
6. S. Bozhevolnyi, E. Bozhevolnaya, and S. Berntsen, "Theoretical model for phase conjugation of optical near fields," J. Opt. Soc. Am. A **12**, 2645–2654 (1995).
7. S. I. Bozhevolnyi and B. Vohnsen, "Near-field optical holography," Phys. Rev. Lett. **77**, 3351–3354 (1996).
8. O. Keller, "Quantum dots of light," J. Nonlinear Opt. Phys. Mater. **5**, 109–132 (1996).
9. S. I. Bozhevolnyi, O. Keller, and I. I. Smolyaninov, "Phase conjugation of an optical near field," Opt. Lett. **19**, 1601–1603 (1994).
10. S. I. Bozhevolnyi and I. I. Smolyaninov, "Characterization of phase-conjugated near-field light spots," J. Opt. Soc. Am. B **12**, 1617–1620 (1995).
11. S. I. Bozhevolnyi, O. Keller, and I. I. Smolyaninov, "Scattered light enhancement near a phase conjugating mirror," Opt. Commun. **115**, 115–120 (1995).
12. Ultramicroscopy **61**, Nos. 1–4 (1995).
13. M. Nieto-Vesperinas and N. García, eds., *Optics at the Nanometer Scale: Imaging and Storing with Photonic Near Fields* (Kluwer, Dordrecht, The Netherlands, 1996).
14. R. C. Reddick, R. J. Warmack, and T. L. Ferrell, "New form of scanning optical microscopy," Phys. Rev. B **39**, 767–770 (1989).
15. D. Courjon, K. Sarayeddine, and M. Spajer, "Scanning tunneling optical microscopy," Opt. Commun. **71**, 23–28 (1989).
16. F. de Fornel, J. P. Goudonnet, L. Salomon, and E. Lesniewska, "An evanescent field optical microscope," in *Optical Storage and Scanning Technology*, T. Wilson, ed., Proc. SPIE **1139**, 77–84 (1989).
17. K. A. Stetson, "Holography with total internally reflected light," Appl. Phys. Lett. **11**, 225–226 (1967).
18. K. A. Stetson, "Improved resolution and signal-to-noise ratios in total internal reflection holograms," Appl. Phys. Lett. **12**, 362–364 (1968).
19. O. Bryngdahl, "Holography with evanescent waves," J. Opt. Soc. Am. **59**, 1645–1650 (1969).
20. O. Bryngdahl, "Evanescent waves in optical imaging," in *Progress in Optics XI*, E. Wolf, ed. (North-Holland, Amsterdam, 1973), Chap. 4.
21. H. Nassenstein, "Superresolution by diffraction of subwaves," Opt. Commun. **2**, 231–234 (1970).
22. D. Van Labeke, D. Barchiesi, and F. Baida, "Optical characterization of nanosources used in scanning near-field optical microscopy," J. Opt. Soc. Am. A **12**, 695–703 (1995).
23. R. Carminati and J.-J. Greffet, "Influence of dielectric contrast and topography on the near field scattered by an inhomogeneous surface," J. Opt. Soc. Am. A **12**, 2716–2725 (1995).
24. A. Sentenac and J.-J. Greffet, "Study of the features of PSTM images by means of a perturbative approach," Ultramicroscopy **57**, 246–250 (1995).
25. D. Van Labeke and D. Barchiesi, "Probes for scanning tunneling optical microscopy: a theoretical comparison," J. Opt. Soc. Am. A **10**, 2193–2201 (1993).
26. D. Van Labeke, F. Baida, D. Barchiesi, and D. Courjon, "A theoretical model for the inverse scanning tunneling optical microscope (ISTOM)," Opt. Commun. **114**, 470–480 (1995).
27. D. Barchiesi and D. Van Labeke, "A perturbative diffraction theory of a multilayer system: applications to near-field optical microscopy SNOM and STOM," Ultramicroscopy **57**, 196–203 (1995).
28. W. Lukosz and R. E. Kunz, "Light emission by magnetic and electric dipoles close to a plane interface. I. Total radiated power," J. Opt. Soc. Am. **67**, 1607–1615 (1977).
29. O. Keller, M. Xiao, and S. Bozhevolnyi, "Configurational resonances in optical near-field microscopy: a rigorous point-dipole approach," Surf. Sci. **280**, 217–230 (1993).
30. C. Girard and A. Dereux, "Near-field optics theories," Rep. Prog. Phys. **59**, 657–699 (1996).
31. D. Gabor, "A new microscopic principle," Nature (London) **161**, 777–778 (1948).
32. D. Gabor, "Microscopy by reconstructed wave-fronts," Proc. R. Soc. London, Ser. A **197**, 454–487 (1949).
33. E. N. Leith and J. Upatnieks, "Reconstructed wavefronts and communication theory," J. Opt. Soc. Am. **52**, 1123–1130 (1962).
34. N. F. van Hulst, F. B. Segerink, F. Achten, and B. Bölger, "Evanescent-field optical microscopy: effects of polarization, tip shape and radiative waves," Ultramicroscopy **42–44**, 416–421 (1992).
35. E. Betzig and J. K. Trautman, "Near-field optics: microscopy, spectroscopy, and surface modification beyond the diffraction limit," Science **257**, 189–195 (1992).